(Received 16 June 2025, Accepted 24 July 2025, Scheduled 6 August 2025)

Stackable Wearable Antenna for Sub-6 GHz Applications: Enhanced Gain and SAR Assessment

Muhammad F. Zambak[1], Ismahayati Adam[2, 3, *], Mohd N. M. Yasin[2, 3], Safbri Johari[2], and Ping J. Soh[4]

[1] *Teknik Elektro, Universitas Muhammadiyah Sumatera Utara, Kota Medan, Sumatera Utara 20238, Indonesia*
[2] *Faculty of Electronic Engineering & Technology, Universiti Malaysia Perlis, Arau 02600, Perlis, Malaysia*
[3] *Centre of Excellence for Advanced Communication Engineering, Universiti Malaysia Perlis, Arau 02600, Perlis, Malaysia*
[4] *Centre for Wireless Communications, University of Oulu, Oulu 90570, Finland*

ABSTRACT: This paper presents the design and performance evaluation of a flexible, multilayer wearable antenna optimized for sub-6 GHz 5G applications at 3.5 GHz. The proposed antenna introduces a fabrication-ready stackable design using textile-compatible materials, including Felt, a 2 mm EVA foam layer, and Shieldit Super. A key innovation lies in the use of low-permittivity EVA foam as an intermediate spacer, which enhances gain and impedance matching without requiring additional structural elements, thus maintaining a compact and mechanically flexible profile. The antenna achieves a peak realized gain of 7.81 dBi and a wide impedance bandwidth of approximately 15.7%, within a total thickness of just 4.34 mm. The design remains robust under bending and close-body scenarios, with specific absorption rate (SAR) analysis confirming compliance with international safety standards. Experimental and simulated results validate the antenna's consistent performance, underscoring its suitability for wearable and Wireless Body Area Network (WBAN) applications in future 5G systems.

1. INTRODUCTION

Body-centric wireless communication systems offer seamless integration into daily wear while maintaining high radiation performance. The use of flexible textile-based substrates such as denim, cotton, and *Shieldit* enables conformability to the human body, but also necessitates careful consideration of mechanical deformation effects, gain enhancement strategies, and compliance with Specific Absorption Rate (SAR) regulations.

Textile-based substrates such as denim, cotton, and *Shieldit* offer excellent flexibility and wearability. However, their low dielectric permittivity (ε) often leads to reduced antenna gain, posing a significant design trade-off between conformability and performance. To overcome this limitation, various gain enhancement strategies have been proposed in recent literature.

Among the widely adopted techniques are Electromagnetic Band Gap (EBG) structures [1, 2] and Artificial Magnetic Conductor (AMC)-integrated reflectors [3–7], which have been demonstrated to improve gain and reduce back radiation [1–7]. These methods not only enhance forward radiation but also contribute to SAR reduction. However, they typically involve multilayered designs and intricate unit-cell patterning, which may increase fabrication complexity and antenna thickness.

Another effective approach involves metasurface and Frequency Selective Surface (FSS)-based structures, which leverage electromagnetic resonance to focus radiation and boost gain [8–11]. In [11], the integration of Reconfigurable Intelligent Surfaces (RIS) with FSS demonstrated a threefold improvement in gain, while [12] reported a gain of 6.85 dBi by embedding grounded metamaterials with high permeability. These methods, although effective, often require precise alignment and complex stacking, which can hinder their suitability for compact and flexible wearable platforms.

Multilayered configurations have also gained traction due to their ability to improve impedance matching and facilitate miniaturization [13–15]. Stacked-layer antennas enhance the effective aperture without increasing the lateral footprint [16]. AMC-backed structures further contribute to gain enhancement and SAR suppression by reflecting surface waves in-phase [6]. Graphene-based conductive multilayers present a promising path, offering both flexibility and excellent electrical performance [17, 18]. Despite these advancements, the complexity and size associated with these designs can limit their practical deployment in low-profile wearable applications.

In contrast to these approaches, the use of a stacked dielectric layer presents a simpler yet effective method to enhance antenna gain. This technique involves inserting an additional textile or flexible dielectric substrate beneath the radiating patch, which increases the effective height of the antenna and supports a more directive radiation pattern. While this leads to a moderate increase in antenna thickness, it avoids the intricacies of AMC or EBG unit cell designs and significantly reduces design and fabrication complexity. Array-based designs are well known to significantly enhance antenna gain, often achieving increases of 20 dBi or more, depending on the array configuration. However, for moderate gain enhancement, the proposed

* Corresponding author: Ismahayati Adam (ismahayati@unimap.edu.my).

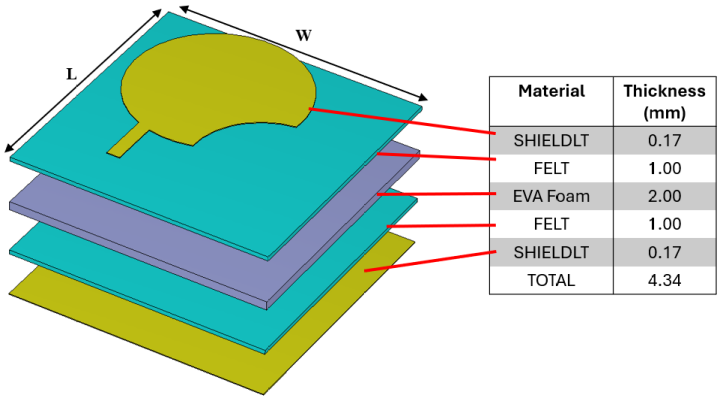

Material	Thickness (mm)
SHIELDLT	0.17
FELT	1.00
EVA Foam	2.00
FELT	1.00
SHIELDLT	0.17
TOTAL	4.34

FIGURE 1. The proposed antenna structure.

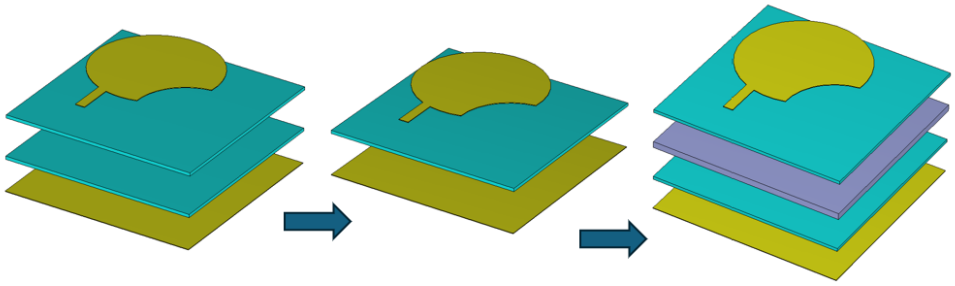

(a) Design 1 (b) Design 2 (c) Design 3

FIGURE 2. Optimization of the antenna, (a) single layer (Design 1), (b) dual substrate layer (Design 2) and (c) triple substrate layer (Design 3).

method offers a more efficient and practical solution, particularly in applications where antenna footprint and mechanical flexibility are critical considerations.

This paper is organized as follows. Section 2 outlines the proposed antenna structure. Section 3 presents a detailed discussion on the antenna design and performance results. The effects of incorporating a multilayer structure are analyzed, with comprehensive evaluations of S_{11}, gain, bending behavior, and SAR performance. Additional wet condition measurements are also included in this section. Finally, the key findings are summarized in Section 4.

2. ANTENNA DESIGN

In this section, the antenna design is described in detail. The proposed design is inspired by a circular patch configuration, incorporating an additional layer to enhance the gain performance. The total antenna size is $60 \times 60 \times 4.34\,\text{mm}^3$.

2.1. The Proposed Structure

The proposed wearable antenna is designed and fabricated using a Felt substrate with a thickness of 1 mm, a relative permittivity (ε_r) of 1.44, and a loss tangent ($\tan(\delta)$) of 0.05. The antenna consists of five layers: the top layer features a truncated circle-shaped radiator made from *Shieldit* Super fabric with a thickness of 0.17 mm, while the bottom layer serves as a full ground plane, also using *Shieldit* Super fabric. A dielectric layer of Felt substrate is used, with a 2 mm EVA foam inserted in the middle of the Felt dielectric to increase the substrate thickness. The proposed antenna is illustrated in Fig. 1.

2.2. Antenna Design and Optimization

In this section, antenna design and simulation were performed to examine the antenna performance and its characteristics. Computer Simulation Technology (CST) Microwave Simulation software was used to design and simulate the antenna performance. Fig. 2 illustrates the antenna optimization process, which begins with a single-layer substrate featuring a truncated circular patch. In this design, the patch and substrate sizes were maintained, while additional layers were incorporated and their effects on antenna performance analysed.

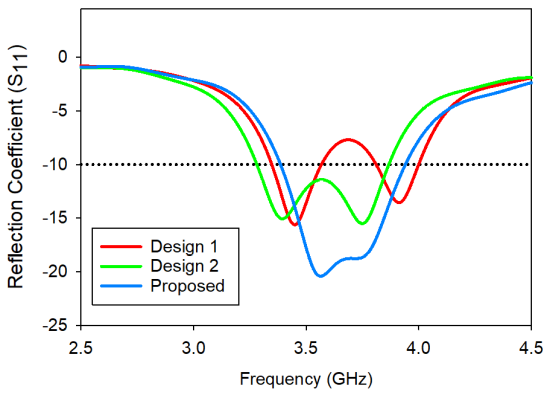

FIGURE 3. The reflection coefficient (S_{11}) at different design stages.

TABLE 1. Details of performance at different stages.

Parameter	S_{11} @3.5 GHz (dB)	BW (GHz)	BW (%)	f_{min}-f_{max} (GHz), f_c (GHz)
Design 1	−13.6	0.22	6.3	3.345–3.57, 3.45 (−15 dB)
Design 2	−12.3	0.57	16.29	3.28–3.869 3.39 (−15 dB)
Proposed Antenna	−17.8	0.55	15.71	3.38–3.94 3.57 (−20.4 dB)

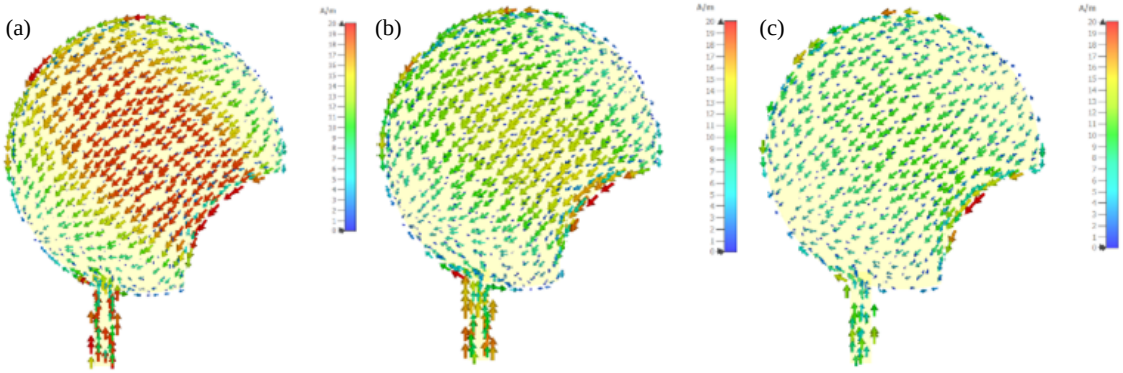

FIGURE 4. Simulated surface current distribution at 3.5 GHz for (a) Design 1 (single layer), (b) Design 2 (dual layer), and (c) proposed antenna (triple layer).

Figure 3 illustrates S_{11} parameters for the three antenna designs. It can be observed that as additional layers are incorporated into the antenna, the impedance matching improves. The additional layers, particularly the Felt-EVA-Felt stack, improve impedance matching by introducing a low permittivity transition layer ($\varepsilon_r \approx 1.1$) between the radiating patch and ground. Furthermore, the S_{11} magnitude deepens, indicating a wider bandwidth. For Design 1, S_{11} experiences some distortion, remaining below −10 dB from 3.45 GHz to 4 GHz, except in the range of 3.57 GHz to 3.80 GHz, where it rises above −10 dB but stays within an acceptable practical limit, below −7 dB. Introducing an extra layer of felt substrate shifts the S_{11} curve to the left, resulting in a 16.3% impedance bandwidth. A detailed performance comparison is provided in Table 1.

The stacked design improves radiation by enhancing current distribution and field behaviour. As shown in Fig. 4, current in the proposed antenna is more uniformly spread and directionally aligned thanthe single- and dual-layer designs. This reduces edge fringing and supports better impedance matching and forward radiation, resulting in higher gain. The increased dielectric height also lowers the Q-factor, broadening bandwidth and improving radiation efficiency.

Meanwhile, adding a 2 mm EVA foam layer deepens the S_{11} to −20 dB, maintaining a 16% impedance bandwidth. Although the proposed antenna design slightly increases the overall height, it significantly improves the gain from 4 dB (Design 2) to 6.93 dB at 3.5 GHz, with a maximum achievable gain of 7.81 dB at 3.7 GHz, as illustrated in Fig. 5.

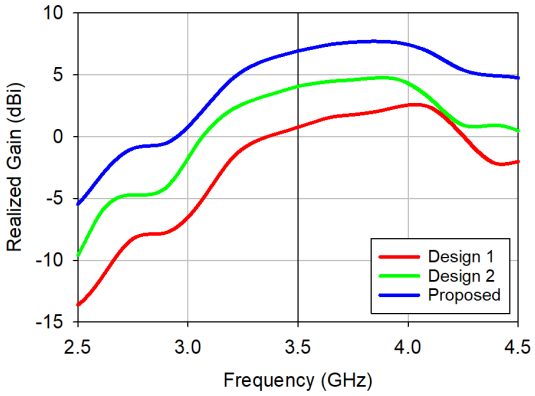

FIGURE 5. The realized gain at different design stages.

3. RESULTS AND DISCUSSION

The results discussed in this section are based on both CST simulations and experimental measurements. A comprehensive evaluation of the antenna performance, including S_{11}, gain, and radiation pattern, is presented, particularly under various bending conditions. Additionally, SAR analysis is included to assess the antenna's suitability for wearable applications.

3.1. The Simulated and Measured S_{11}

Figure 6 shows the fabricated prototype of the proposed antenna, where the antenna S_{11} was measured using Vector Network Analyzer (VNA) from Keysight as in Fig. 6(c) and the wet

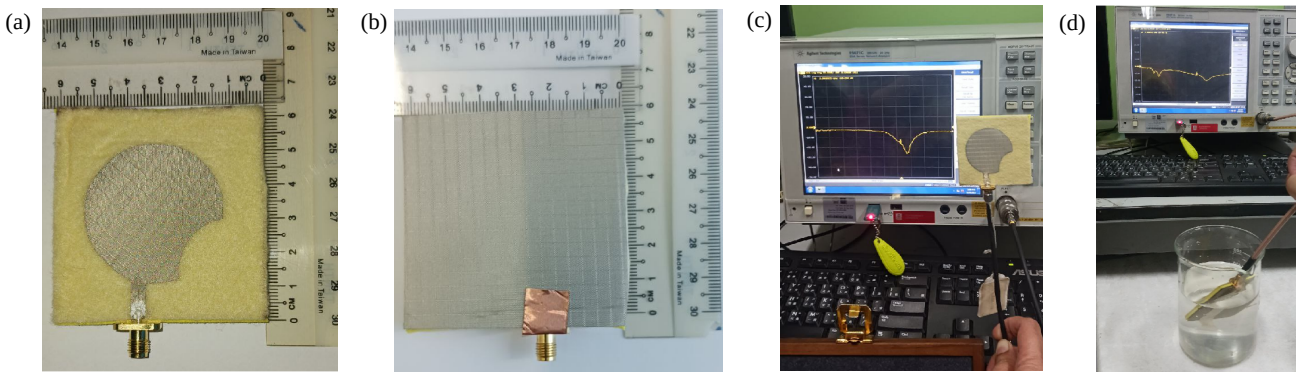

FIGURE 6. The fabricated structure. (a) Front view, (b) back view, (c) S_{11} measurement (flat) and (d) wet measurement.

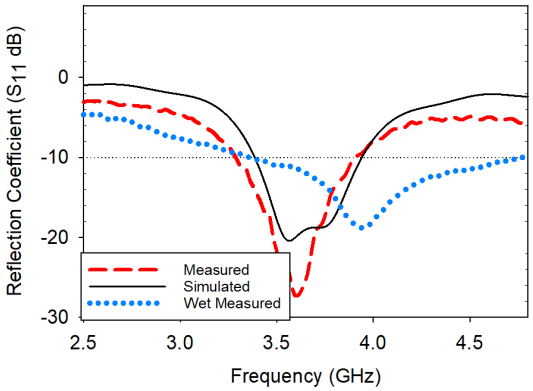

FIGURE 7. The simulated and measured S_{11}.

measurement shown in Fig. 6(d). The graph illustrates in Fig. 7 is the S_{11} comparing simulated, measured, and wet measured results. The simulated response, represented by the black solid line, shows a clear resonance around 3.5 GHz, where the S_{11} reaches a minimum below -20 dB, indicating good impedance matching and efficient radiation at that frequency. The measured response, depicted by the red dashed line, closely follows the simulated trend, but with a slight shift in the resonance and a higher minimum S_{11} value around -25 dB. These deviations could be attributed to fabrication tolerances, material inconsistencies, or measurement setup variations. In contrast, the wet measured response, shown by the blue dotted line, demonstrates a noticeable shift in the resonance frequency and an overall increase in S_{11} values across the spectrum. The minimum S_{11} in wet condition reaches only about -15 dB, suggesting that moisture adversely impacts the antenna's performance, likely due to changes in the dielectric properties that result in impedance mismatch. However, the S_{11} response remains below -10 dB at 3.5 GHz, indicating that the antenna is still operational at this frequency despite the presence of moisture.

3.2. The Simulated and Measured Radiation Pattern

The radiation characteristics of the proposed antenna were analyzed through both simulation and measurement, with results presented in Fig. 8. Fig. 8(a) shows the measurement setup inside an anechoic chamber, where a horn antenna is used to transmit the signal. The radiation patterns were evaluated in the XZ-plane and YZ-plane, corresponding to Fig. 8(b) and Fig. 8(c), respectively. The simulated patterns, represented by the solid black lines, exhibit a relatively omnidirectional behavior, while the measured patterns, depicted by the red dashed lines, generally follow the simulated trends but display some discrepancies, particularly in the lower hemisphere (angles between 180° and 270°). These deviations may be attributed to fabrication tolerances and environmental interferences. Despite these variations, the measured results confirm the expected radiation performance, demonstrating that the antenna maintains stable radiation characteristics across both principal planes.

3.3. Bending Analysis

Bending analysis is a critical aspect of wearable antenna design. The robustness of the antenna under mechanical deformation can be evaluated by subjecting it to various bending curvatures. Fig. 9(a) illustrates the simulated 3D radiation pattern of the antenna under a bent condition, while Fig. 9(b) shows the measurement setup used for the bending analysis. In this analysis, the antenna was tested with bending radii ranging from flat ($D = \infty$ mm) to 40 mm.

As the bending decreases from flat to 40 mm, the resonance frequency undergoes a slight shift, and the S_{11} performance varies. The flat and larger bending radii (100 mm and 80 mm) exhibit good agreement between simulation and measurement, with S_{11} values remaining well below -10 dB around the resonance frequency. However, tighter bending conditions (60 mm and 40 mm) result in more noticeable discrepancies, including resonance shifts and reduced return loss depth, particularly in the measured results, depicted in Fig. 10.

Summarized in Table 2, the simulated impedance bandwidths are maintained above 500 MHz, while in measurement, the bandwidths are reduced by approximately 100 MHz due to the effects of bending. Despite these variations, all bending conditions still demonstrate acceptable performance. In terms of gain, bending the antenna reduces its peak gain from 7 dBi (flat condition) to approximately 6 dBi at 3.5 GHz, indicating a moderate impact on radiation efficiency due to mechanical deforma-

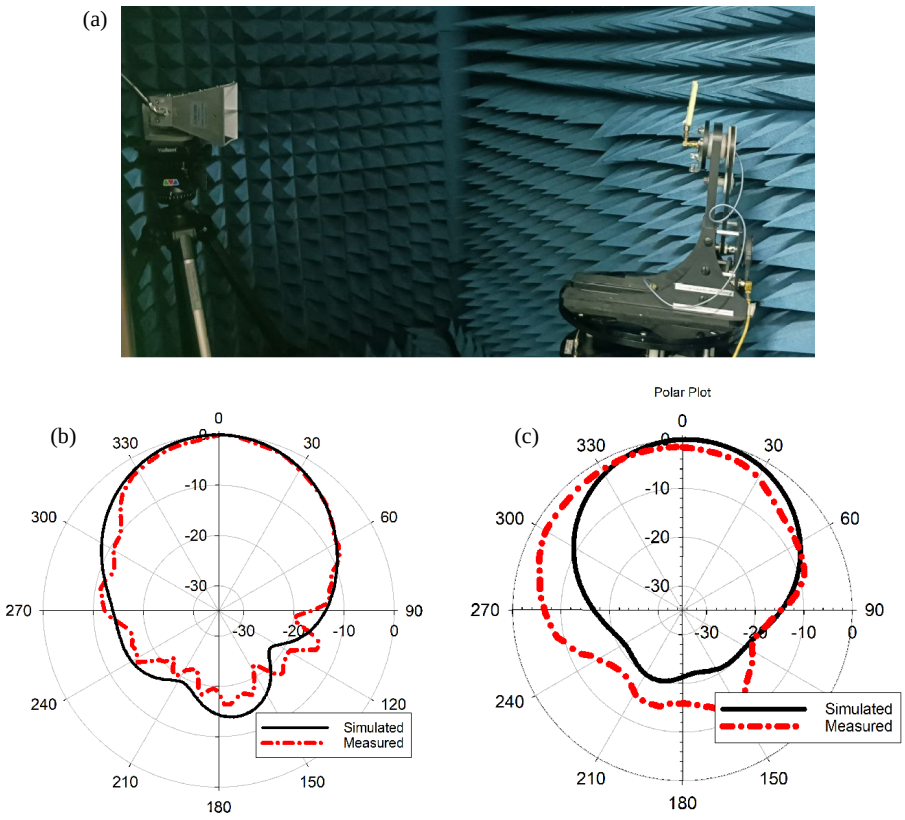

FIGURE 8. (a) The measurement setup in anechoic chamber and (b) X-Z plane, (c) Y-Z plane is the simulated and measured radiation pattern.

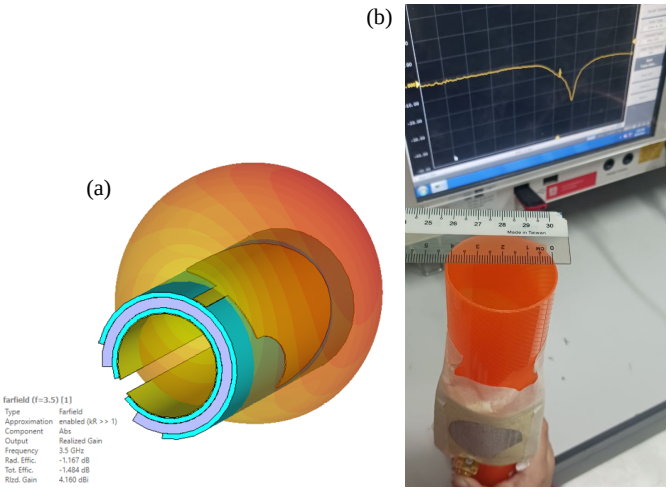

FIGURE 9. Antenna structure under bending condition: (a) Simulated 3D radiation pattern while bent, and (b) measurement setup for bending evaluation.

tion. Additionally, the radiation pattern remains largely stable, with the main lobe direction preserved and only minor angular deviations of 1° to 2°, as illustrated in Fig. 11.

Front-to-Back Ratio (FBR) was analysed to quantify the level of backward radiation, which serves as a critical metric for evaluating the antenna's directional performance and its safety in proximity to the human body. The FBR values were extracted at 3.5 GHz under both flat and various bending conditions to simulate realistic on-body deformations. As presented in Table 3, the FBR consistently remains above 1.68 dB across all tested scenarios, with the highest value reaching 1.98 dB at a bending diameter of $D = 40$ mm. This result indicates effective suppression of backward radiation, demonstrating the antenna's suitability for wearable applications.

TABLE 2. Simulated and measured S_{11} performance at different bending radii.

	Parameter	Flat	100	80	60	40
Sim	$f_{\min}$ (GHz)	3.39	3.40	3.42	3.41	3.41
	$f_{\max}$ (GHz)	3.94	3.96	3.96	3.98	3.95
	Bw (MHz)	554	551	544	570	546
	f_c (GHz)	3.56	3.57	3.6	3.59	3.56
	S_{11} (dB)	−16	−16.1	−16.4	−15.6	−20.4
Meas	$f_{\min}$ (GHz)	3.32	3.4	3.42	3.36	3.38
	$f_{\max}$ (GHz)	3.9	3.8	3.9	3.8	3.9
	Bw (MHz)	580	400	480	460	520
	f_c (GHz)	3.6	3.64	3.68	3.68	3.72
	S_{11} (dB)	−27	−15.1	−23.3	−21.6	−27.9

3.4. Antenna Analysis on Body Phantom

Wearable antennas are typically used in close proximity to the human body. To accurately simulate this real-world scenario, a four-layer human tissue phantom was modeled in CST at the

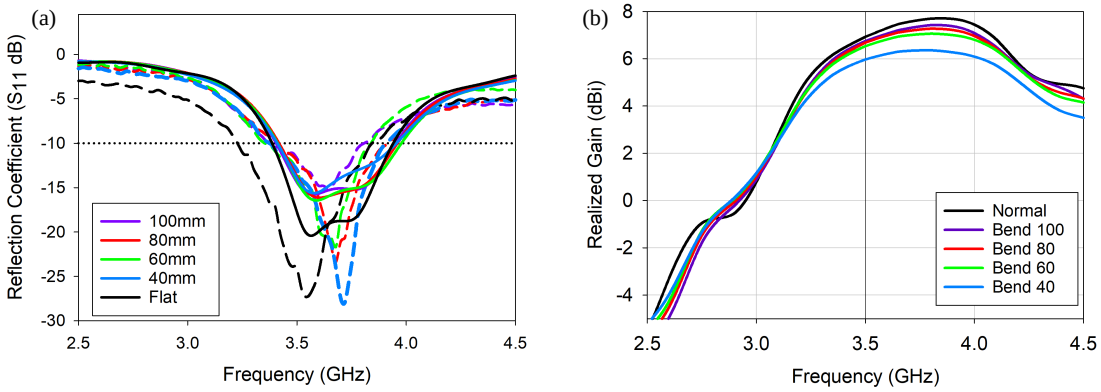

FIGURE 10. (a) The S_{11} for simulated and measured at different bending radius and (b) the simulated gain of different bending radii.

TABLE 3. Simulated Front-to-Back Ratio (FBR) at 3.5 GHz for various bending diameters compared to the flat configuration.

Bending Radius	FBR (dB) at 3.5 GHz
No bend	1.93
$D = 140$ mm	1.92
$D = 120$ mm	1.72
$D = 100$ mm	1.68
$D = 80$ mm	1.96
$D = 60$ mm	1.73
$D = 40$ mm	1.98

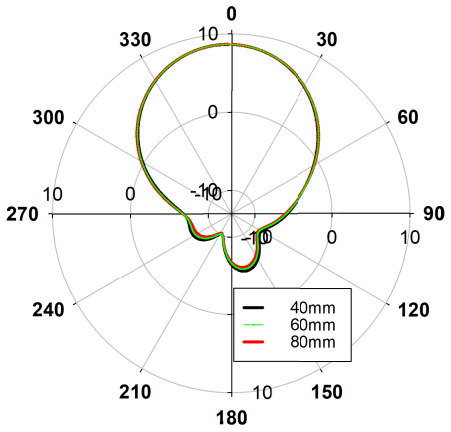

FIGURE 11. The polar radiation pattern for different bending radii.

target frequency of 3.5 GHz. The defined tissue layers represent realistic body composition and are detailed in Table 4.

The plot in Fig. 12 illustrates the S_{11} and realized gain performance of the proposed antenna when being subjected to various bending radii in the presence of a body phantom. As the antenna is bent with decreasing radii — 120 mm, 100 mm, 80 mm, 60 mm, and 40 mm — a noticeable shift in the resonance frequency occurs, moving slightly lower to around 3.4 GHz. Additionally, the impedance bandwidth (BW) also increases for radius of 80 mm and above, suggesting enhanced performance under moderate bending. Overall, the antenna maintains an S_{11} better than -10 dB across all tested bending conditions with the body phantom, down to a minimum radius of 40 mm, indicating

TABLE 4. Tissue bodies at 3.5 GHz.

Tissue	Thickness (mm)	ε_r	σ
Skin	2	37.003	2.025
Fat	8	5.174	0.155
Muscle	23	52.939	2.794
Bone	10	10.793	0.614

TABLE 5. SAR values at 1 g and 10 g tissue with different bending radii.

Condition/SAR	1 g	10 g
No bend	1.028	0.273
$D = 120$ mm	1.453	0.325
$D = 100$ mm	1.688	0.535
$D = 80$ mm	1.590	0.459
$D = 60$ mm	1.385	0.318
$D = 40$ mm	1.247	0.327

robust operation under deformation. Furthermore, the realized gain gradually decreases with tighter bending, reducing from 7 dBi at 120 mm to 5.88 dBi at 40 mm, likely due to increased deformation and interaction with the phantom.

Figure 13 illustrates the radiation pattern of the proposed antenna in both flat and bent conditions, in the presence of a body phantom. It can be observed that the antenna primarily radiates in the forward direction, which is desirable for Wireless Body Area Network (WBAN) applications, as it minimizes radiation toward the body. The presence of bending does not significantly alter the direction of the main lobe, with only a slight shift of approximately 1° to 2° observed.

3.5. Antenna Analysis on Body (SAR Analysis)

Another key parameter for evaluating the performance of the wearable antenna is the SAR analysis. SAR quantifies the amount of RF energy absorbed by human tissues when they are exposed to electromagnetic fields, as shown in (1).

$$\mathrm{SAR} = \frac{\sigma |E|^2}{2\rho} \tag{1}$$

TABLE 6. Performance comparison between the proposed antenna and those from the literature.

Ref.	Overall Size (λ^3/mm)	f (GHz)	BW (%)	Gain (dBi)	Method
[2]	$0.8\lambda_0 * 0.8\lambda_0 * 0.05\lambda_0$ $69 \times 69 \times 2\,\text{mm}^3$	3.5	16	6.43	CPW + EBG
[3]	$0.7\lambda_0 * 0.7\lambda_0 * 0.2\lambda_0$ $60 \times 60 \times 17\,\text{mm}^3$	3.5	*NA	7.53	AMC
[6]	$\lambda_0 * \lambda_0 * 0.07\lambda_0$ $86 \times 86 \times 6\,\text{mm}^3$	3.5 & 5.8	33	9.078	AMC
[7]	$0.8\lambda_0 * 0.8\lambda_0 * 0.1\lambda_0$ $40.5 \times 40.5 \times 6\,\text{mm}^3$	5.86	15.5	7.47	AMC
[11]	$1\lambda_0 * 1\lambda_0 * \lambda_0/2$ $73 \times 73 \times 36.5\,\text{mm}^3$	5.7	17.72	12.48	FSS + RIS
Propose	$0.7\lambda_0 * 0.7\lambda_0 * 0.05\lambda_0$ $60 \times 60 \times 4.34\,\text{mm}^3$	3.5	15.71	6.83	stacked

*NA — not mention in paper.

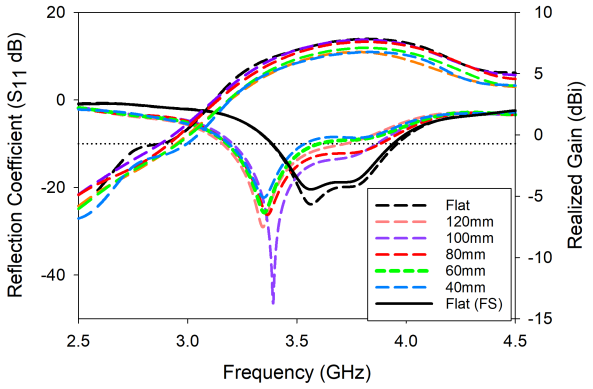

FIGURE 12. S_{11} performance for antenna with body phantom at different bending radii.

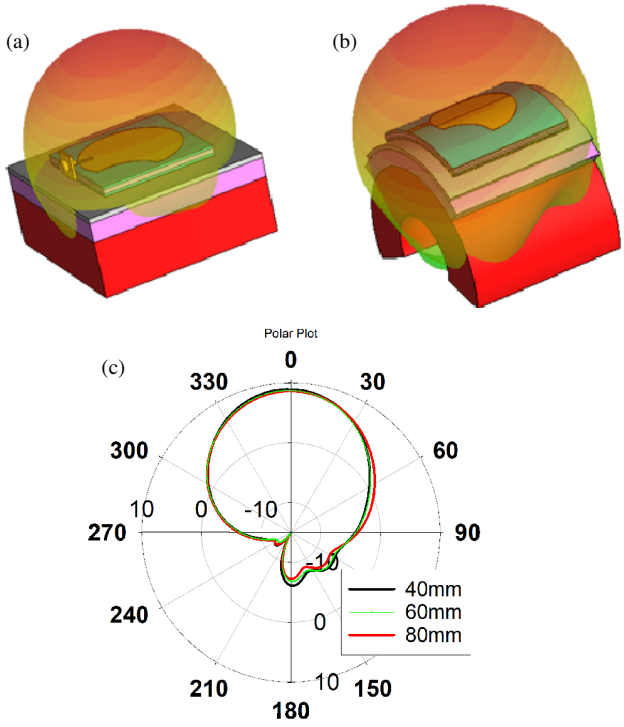

FIGURE 13. (a), (b) 3D radiation pattern for antenna with phantom. (c) 2D polar radiation pattern with phantom.

where σ is the electrical conductivity of the tissue (in S/m), E the electric field strength inside the tissue (in V/m), and ρ the mass density of the tissue (in kg/m^3). Regulatory bodies such as the FCC (USA) and ICNIRP (Europe) have set SAR limits to ensure user safety, with the FCC imposing a 1.6 W/kg limit averaged over 1 g of tissue, while ICNIRP allows 2.0 W/kg to average over 10 g of tissue. These limits help mitigate excessive heating and potential biological effects of prolonged radio frequency (RF) exposure. In the analysis, bending conditions were also considered for both 1 g and 10 g body tissues.

Figure 14 illustrates the simulated SAR distribution for the proposed antenna under both flat and bent conditions. Table 5 summarizes the SAR values evaluated at different bending radii and under two mass averaging conditions: 1 g and 10 g. The SAR results in Table 5 reveal that the maximum SAR occurs at a bending radius of 100 mm, reaching 1.688 W/kg under 1 g and 0.535 W/kg under 10 g. Interestingly, further tightening the curvature to 80 mm, 60 mm, and 40 mm results in a progressive decline in SAR values. This trend aligns well with the reflection coefficient and gain characteristics shown in Fig. 12, where the antenna at 100 mm exhibits the best impedance matching and highest realized gain. Tighter bends introduce detuning and slight performance degradation, as seen from increased S_{11} and reduced gain.

In the 1 g condition, SAR reaches its peak at $D = 100$ mm (1.688 W/kg) before decreasing as the curvature increases further. Similarly, in the 10 g condition, the highest SAR is observed at $D = 100$ mm (0.535 W/kg), indicating greater absorption in this specific bending configuration. This reduction may be attributed to changes in tissue properties, variations in antenna-body interactions, or altered impedance matching.

Figure 15 illustrates the SAR distribution of the proposed antenna evaluated on a Hugo human phantom, with the antenna

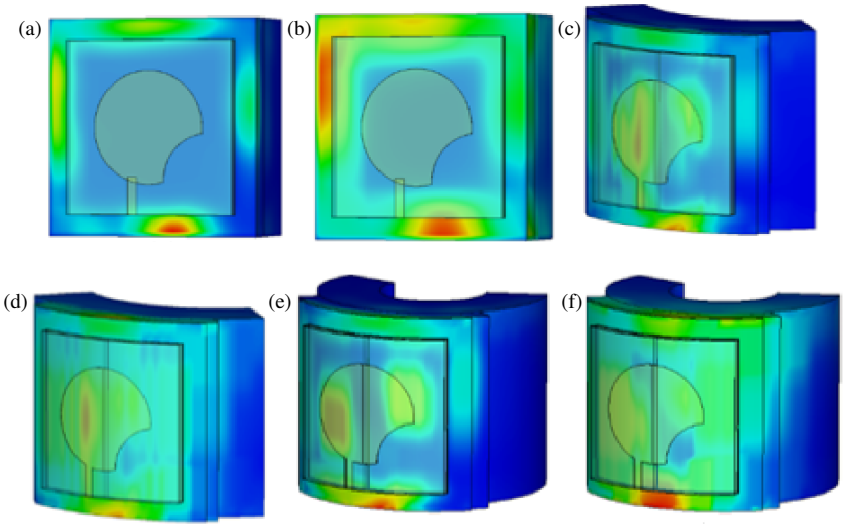

FIGURE 14. SAR distribution of the proposed antenna under different bending radii on flat tissue. (a), (b) Flat placement (1 g, 10 g), (c), (d) bent at $D = 100$ mm (1 g, 10 g) and (e), (f) bent at $D = 40$ mm (1 g, 10 g).

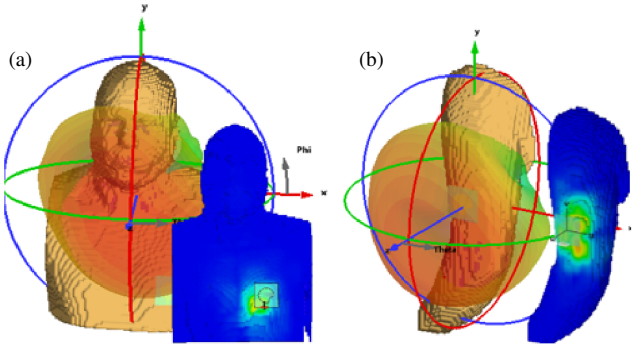

Condition	1g (W/kg)	10g (W/kg)
Chest	0.855	0.402
Hand	0.319	0.157

FIGURE 15. SAR analysis of the proposed antenna on the Hugo phantom (a) on chest and (b) on left hand.

positioned 5 mm from the body surface. Fig. 15(a) shows the SAR distribution when the antenna is placed on the chest, while Fig. 15(b) corresponds to placement on the left hand. The table presents the peak SAR values averaged over 1 gram and 10 grams of tissue for both locations. When being mounted on the chest, the antenna exhibits SAR values of 0.855 W/kg (1 g) and 0.402 W/kg (10 g), whereas placement on the hand yields lower SAR values of 0.319 W/kg (1 g) and 0.157 W/kg (10 g). These results indicate that the electromagnetic absorption is higher near the chest due to the proximity of vital organs and denser tissues. Nevertheless, all measured SAR values remain well below international safety thresholds, demonstrating that the proposed design, with its grounded metamaterial configuration, effectively minimizes electromagnetic exposure and ensures safe operation for wearable applications.

The performance of the proposed antenna is compared with existing literature on wearable antenna designs focused on gain enhancement, as illustrated in Table 6. Among the commonly used techniques, AMC structures are the most prevalent for improving gain, followed by EBG structures, FSS, and metamaterials. It is important to note that the comparison is based on simulated gain values reported in respective studies. Of particular interest, the proposed antenna achieves comparable gain enhancement using a simpler approach which is by introducing an additional layer between the substrates, demonstrating similar performance levels to those reported in more complex designs.

4. CONCLUSION

This paper has presented the design, simulation, and experimental validation of a multilayer wearable antenna tailored for sub-6 GHz 5G applications. The proposed antenna, built using a felt substrate and integrated with EVA foam, demonstrates enhanced impedance bandwidth and gain performance, with a peak realized gain of 7.81 dBi at 3.7 GHz. The multilayer approach effectively improves performance while maintaining flexibility and a compact profile, making it suitable for wearable applications. Notably, the antenna maintains its operating frequency even when being submerged in water, demonstrating robust environmental resilience. Comprehensive evaluations under bending conditions and with a realistic four-layer body phantom reveal that the antenna maintains stable S_{11} characteristics and directional radiation behaviour, even under deformation. Additionally, SAR analysis confirms that the design remains within international safety limits for both 1 g and 10 g tissue models. Overall, the proposed antenna offers a reliable, efficient, and mechanically robust solution for next-generation wearable communication systems, particularly in Wireless Body Area Network (WBAN) environments.

ACKNOWLEDGEMENT

The authors would like to acknowledge the support from the International Research Fund (INTERES) 9001-00746.

REFERENCES

[1] Li, R., C. Wu, X. Sun, Y. Zhao, and W. Luo, "An EBG-based triple-band wearable antenna for WBAN applications," *Micromachines*, Vol. 13, No. 11, 1938, 2022.

[2] El May, W., I. Sfar, J. M. Ribero, and L. Osman, "Design of low-profile and safe low SAR tri-band textile EBG-based antenna for IoT applications," *Progress In Electromagnetics Research Letters*, Vol. 98, 85–94, 2021.

[3] Badisa, A., B. T. Madhav, K. Srilatha, M. C. Rao, and S. Das, "A circularly polarized quad-band wearable textile antenna integrated with triple band AMC reflector for WBAN applications," *Progress In Electromagnetics Research C*, Vol. 121, 1–18, 2022.

[4] Aitbar, I., N. Shoaib, A. Alomainy, A. Quddious, S. Nikolaou, M. A. Imran, and Q. H. Abbasi, "AMC integrated multilayer wearable antenna for multiband WBAN applications," *Computers, Materials and Continua*, Vol. 71, No. 2, 3227–3241, 2022.

[5] Alemaryeen, A. and S. Noghanian, "On-body low-profile textile antenna with artificial magnetic conductor," *IEEE Transactions on Antennas and Propagation*, Vol. 67, No. 6, 3649–3656, 2019.

[6] El Atrash, M., M. A. Abdalla, and H. M. Elhennawy, "A wearable dual-band low profile high gain low SAR antenna AMC-backed for WBAN applications," *IEEE Transactions on Antennas and Propagation*, Vol. 67, No. 10, 6378–6388, 2019.

[7] Saha, P., D. Mitra, and S. K. Parui, "Control of gain and SAR for wearable antenna using AMC structure," *Radioengineering*, Vol. 30, No. 1, 81–88, 2021.

[8] Çelenk, E. and N. T. Tokan, "All-textile on-body metasurface antenna," *Progress In Electromagnetics Research M*, Vol. 110, 119–131, 2022.

[9] Le, T. T. and T.-Y. Yun, "Wearable dual-band high-gain low-SAR antenna for off-body communication," *IEEE Antennas and Wireless Propagation Letters*, Vol. 20, No. 7, 1175–1179, 2021.

[10] Aishwarya, T. and P. Das, "A FSS integrated wearable modified bow-tie antenna for biomedical applications," *Results in Engineering*, Vol. 26, 104894, 2025.

[11] Srinivas, G. and D. Vakula, "High gain and wide band antenna based on FSS and RIS configuration," *Radioengineering*, Vol. 30, No. 1, 96–103, 2021.

[12] Das, G. K., S. Basu, B. Mandal, D. Mitra, R. Augustine, and M. Mitra, "Gain-enhancement technique for wearable patch antenna using grounded metamaterial," *IET Microwaves, Antennas & Propagation*, Vol. 14, No. 15, 2045–2052, 2020.

[13] Alzahrani, S., "A wideband 2×2 stacked antenna array with 9.5 dBi gain for MMW applications," in *2024 11th International Conference on Electrical Engineering, Computer Science and Informatics (EECSI)*, 396–398, Yogyakarta, Indonesia, Sep. 2024.

[14] Natali, Y. and M. Larasati, "Gain enhancement using stub and stacked hexagon microstrip antenna for 5G communication," in *2019 International Conference on Radar, Antenna, Microwave, Electronics, and Telecommunications (ICRAMET)*, 49–52, Tangerang, Indonesia, 2019.

[15] Lv, J., X. Xu, and B. Zhang, "Probe-fed wideband planar phased array antenna element using stacked rectangular and U-slot patches in low vertical profile," in *2022 IEEE International Workshop on Electromagnetics: Applications and Student Innovation Competition (iWEM)*, 182–183, Narashino, Japan, 2022.

[16] Fitra, M., I. Adam, M. N. M. Yasin, N. Haris, N. M. Nawawi, and A. S. M. Zain, "Miniaturization of stacked wearable antenna for 5G applications," *Jurnal Teknologi (Sciences & Engineering)*, Vol. 86, No. 5, 137–144, 2024.

[17] Al-Gburi, A. J. A., M. M. Ismail, N. J. Mohammed, and T. A. H. Alghamdi, "SAR flexible antenna advancements: Highly conductive polymer-graphene oxide-silver nanocomposites," *Progress In Electromagnetics Research M*, Vol. 127, 23–30, 2024.

[18] Xiao, Y., H. Zu, R. Song, Y. Xin, Y. Xi, G.-L. Huang, B. Wu, and D. He, "Multiband and low-specific-absorption-rate wearable antenna with low profile based on highly conductive graphene assembled film," *IEEE Antennas and Wireless Propagation Letters*, Vol. 22, No. 9, 2195–2199, 2023.